

Antigen-driven clonal selection shapes the persistence of HIV-1 infected CD4⁺ T cells *in vivo*

Francesco R. Simonetti, Hao Zhang, Garshasb P. Soroosh, Jiayi Duan, Kyle Rhodehouse, Alison L. Hill, Subul A. Beg, Kevin McCormick, Hayley Raymond, Christopher L. Nobles, John Everett, Kyungyo J. Kwon, Jennifer A. White, Jun Lai, Joseph B. Margolick, Rebecca Hoh, Steven G. Deeks⁵, Frederic D. Bushman, Janet D. Siliciano, Robert F. Siliciano.

Supplementary Materials

Supplementary Results. Characterization of proviral sequences in antigen-responding clones.

Supplementary Methods.

Supplementary Figure S1. Accessing antigen-responding CD4+ T cells.

Supplementary Figure S2. Longitudinal sampling schema and experiments performed at each time point.

Supplementary Figure S3. Validation experiment of whole genome amplification on sorted JLat cells

Supplementary Figure S4. Summary of identical HIV-1 DNA single genome sequences recovered from sorted cells.

Supplementary Figure S5. Proviral structures with large deletions and aberrant provirus/host junctions.

Supplementary Figure S6. Intact proviral DNA assay analysis of individual proviruses.

Supplementary Figure S7. Quantitative viral outgrowth assay data from sorted CD4+ T cells.

Supplementary Figure S8. Additional analyses on TCR β sequences.

Supplementary Figure S9. Pairing of TCR β sequences and proviruses belonging to the same clonotype.

Supplementary Figure S10. Contribution of CD4+ T cell subsets to antigen-responsive clonotypes carrying HIV proviruses.

Supplementary Table S1. Participant characteristics.

Supplementary Table S2. Single genome sequences and oligoclonality of proviral populations from sorted CD4+ T cells.

Supplementary Table S3. Integration site analysis of HIV-1-infected antigen-responding clones.

Supplementary Table S4. Characteristics of TCR β sequences in clusters shown in Figure 4.

Supplementary Table S5. Likelihoods that clones would reach the observed sizes under a model of homeostatic proliferation.

Supplementary Table S6. Primers and probes used in this study (xml file).

Supplementary Table S7. High resolution HLA genotyping of the study participants.

Supplementary Results

Characterization of proviral sequences in antigen-responding clones.

To investigate whether clones of HIV-1-infected, Ag-responding cells carried intact or defective proviruses, we recovered the partial or full-length sequences of the proviruses for which we identified integration sites (Figures 3A and C). As expected, most genomes (13/22) were defective due to deletions that we either mapped (8/22) or inferred (5/22) due to failure of PCR amplification or lack of signal from one amplicon in the Intact Proviral DNA assay (IPDA, see below). Of the remaining defective proviruses, seven showed G-to-A hypermutation and one had a 93-nucleotide deletion affecting the dimerization, major splicing donor, and packaging signal stem loops (P5, integrated in *DELEC1*). Only one provirus had no defects that would abrogate infectivity (found in participant P3, integrated in *FXBO22*).

In some cases, primers commonly used for near full-length proviral sequencing (27, 97, 98) failed due to deletions. Therefore, we used the integration site to design primers in host DNA flanking the host-proviral junctions. This allowed recovery of near full genome sequences from 5 proviruses (integrated in *ST6GALNAC3*, *KCNC2* and 3 proviruses in *BACH2*, respectively) with unusual proviral structures (Figure S5). These proviruses had large deletions (range 3749-7335 nucleotides) almost completely encompassing one of the LTRs (Figures 3A and S5). For two of these proviruses, the deletion extended outside the HIV-1 genome, and the 5-nucleotide duplication typically left by the integration process (99) was absent, suggesting that these proviruses might be the result of aberrant integration (100, 101). These observations reflect the striking heterogeneity of the proviral landscape, which is challenging to analyze without PCR bias. Two of these proviruses (integrated in *ST6GALNAC3* and outside of *KCNC2*) belonged to the most abundant infected clones in the study but would have been missed with standard full-genome sequencing.

We also analyzed whole genome amplified DNA using the IPDA, a novel droplet digital PCR assay that uses two strategically placed amplicons to distinguish intact from defective proviruses (81). The IPDA allowed assessment of the intactness of these clonally expanded proviruses in case of incomplete recovery of genome sequences (Figure 3A). In addition, for 17 completely sequenced proviruses, the IPDA signal pattern showed 100% agreement with patterns expected based on the sequencing data (Figure S6).

Supplementary Methods

Quantification of specific proviruses and VDJ rearrangements. To quantify proviruses of interest together with the VDJ rearrangement of their cognate clonotypes, we used the droplet digital PCR platform QX200 (Bio-Rad). In order to prevent non-specific amplification of unrelated proviral sequences, we designed primers across the host-U3 or U5-host junctions. In addition, the fluorescently labelled probe was designed to anneal across the site of HIV-1 integration. In case of proviruses integrated in regions with repetitive sequences or with a GC content unsuitable for primer design, we designed primers and probes across large internal deletions that were unique to the provirus of interest. Similarly, for primers and probes aimed to quantify specific VDJ regions, we placed the forward and reverse primers on the V and J regions, respectively, and the probe was designed to span the junctions between the V-D-J regions, in order to exploit N and P nucleotides and small deletions randomly occurring during the recombination process. PCR reactions were run with the following parameters: 95°C for 10', 95°C for 30s, 56°C for 2' (steps 2 to 3 for 44 cycles), 98°C for 10', hold at 4°C (temperature change rate 2°C/s). Primers and probe had a final concentration of 900nM and 250nM, respectively. The specificity of each set was tested against a panel of whole genome amplified DNA samples with and without the CD4⁺ T cell clones of interest and a sample of CD4⁺ T cell derived gDNA from healthy donors. Primers are probes are shown in Supplementary Table S6. We performed parallel quantification of RPP30 as previously described (81) to calculate cell equivalents and normalized copies of proviral integration sites and VDJ rearrangements.

Assignment of TCR-provirus pairs from Antigen-reactive clonotypes. To pair the TCR β of an antigen-responsive CD4⁺ cells and the provirus integrated in the same clonotype, we leveraged TCR diversity and combinatorial statistics previously used to confidently pair TCR α and β chains (56). Briefly, a fixed number of antigen-reactive cells are randomly allocated to each well on a 96-well plate and subjected to WGA as described above. TCR β immunosequencing is performed on wells sharing the same proviral sequence and integration site and TCR β sequences recurring in all wells are considered as candidate for pairing experiments. Subsequently, the whole plate is screened by duplex ddPCR with assays design to specifically detect both the integration site and the candidate TCR β sequence. Given that immune repertoire is highly diverse, even within antigen-responsive cells, the probability that a specific TCR β sequence and a provirus will occupy exactly the same sets of wells is minuscule, so a pair of TCR β and proviral sequences that uniquely share a set of wells can be inferred to have come from the same clone. For each potential TCR β /provirus pair, we computed a P value for the observed number of shared wells, implementing the calculations described by Howie *et al.* (56) shown in supplementary Figure S9A and B.

Total body size estimates and likelihood of homeostatic proliferation. To estimate the total body size of HIV-1-infected CMV-responding clones, we used the frequency of infected cells carrying the relevant provirus among all CMV-responding CD4⁺ T cells, as quantified with the provirus-specific ddPCR assays. We then used the percentage of CMV-responding CD4⁺ T cells upon antigen stimulation to extrapolate the frequency of the relevant clone among all CD4⁺ T cells. Total body cell number (2¹¹) was estimated based on the average CD4⁺ T cell counts in individuals on long-term ART (17, 18, 27) (800 cell/ μ L), the fraction of cells in circulation (102) (0.02) and the average total blood volume (5L). The number of divisions needed to reach the observed clone sizes is calculated with the Log₂ of the total body size of each infected clone (Supplementary Table S5). Of note, this assumes no cell death (a clone can only divide). We then calculated the likelihood a clone could reach this size if the entire population of CD4⁺ T cells was maintained by a constant, balanced, process of division and death (only random events lead clones to grow or shrink). We applied a range of proliferation rates (10-1000 divisions/year) to represent cell subsets with different proliferative potential (i.e. naïve vs resting memory vs activated effector cells). Calculations were conducted with two scenarios, one with the expected reservoir decay (4)(5) (44 months) and one with no net decay (103) (defective or total HIV-DNA). The death rate (d) was calculated so that the difference between the proliferation rate (p) and the death rate was equal to the observed net decay rate ($\delta = p - d$). The probability of observing a clone of size X or larger with these turnover parameters was calculated using the formula

$$\bar{F}(X; t, p, d) = \begin{cases} 1 & X = 0 \\ (1 - \alpha)\beta^{X-1} & X > 0 \end{cases}$$

With

$$\alpha = \frac{de^{\delta t} - d}{pe^{\delta t} - d},$$

$$\beta = \frac{pe^{\delta t} - p}{pe^{\delta t} - d}$$

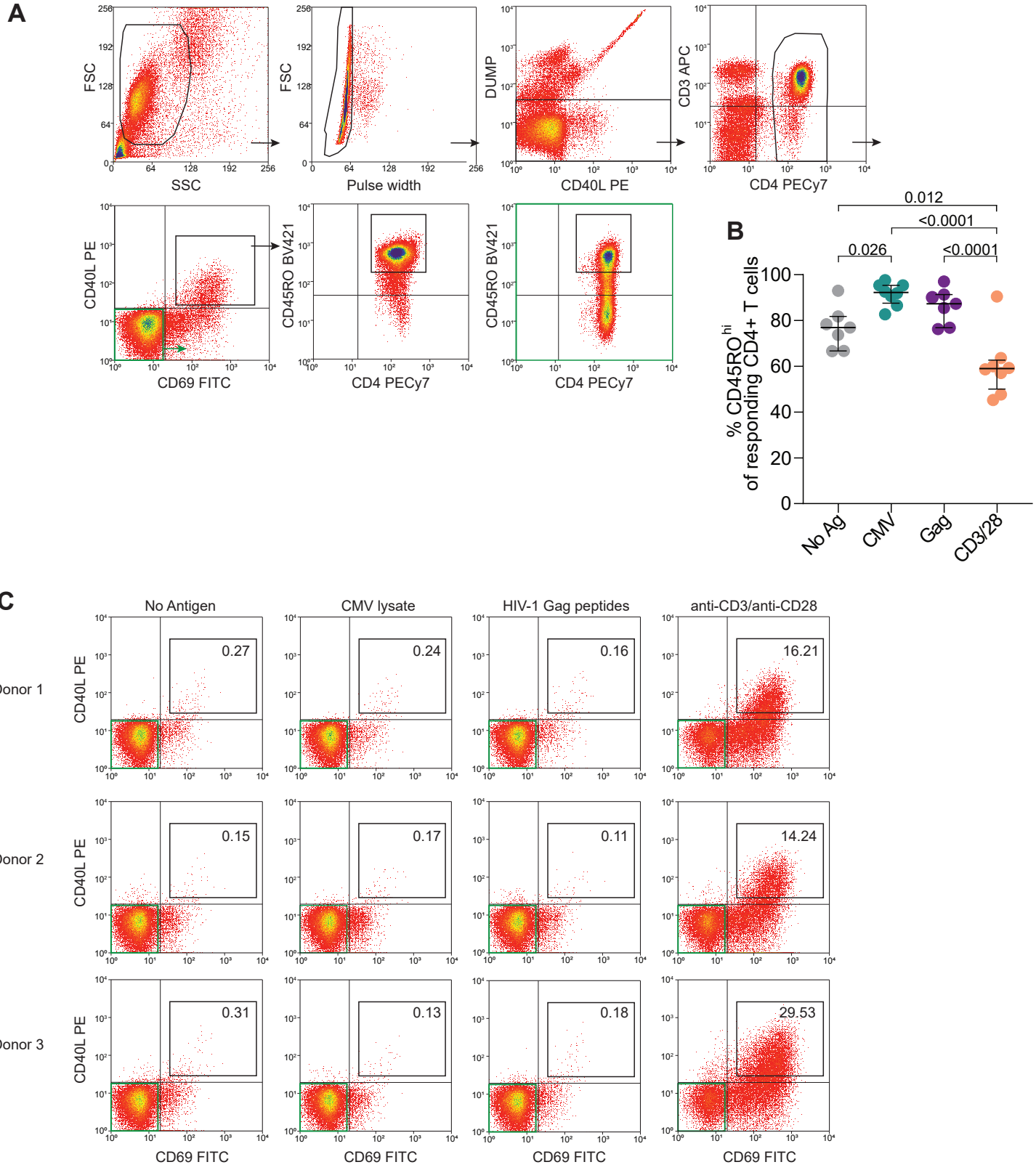
which is the complementary cumulative distribution function for the solution of a homogeneous birth-death process starting with a single cell at time zero (104). We take time zero to be the time for viral suppression to < 50 copies per mL, which means we assume that proliferation predominantly occurs after viral suppression. If there are N unique clones in the body, then the likelihood of observing at least one clone that is at least size X is

$$\mathcal{L}(X; t, p, d) = 1 - (1 - \bar{F}(X; t, p, d))^N \approx N\bar{F}(X; t, p, d)$$

where the approximation holds as long as $\bar{F}(X; t, p, d) \ll 1$. We assume that at the time of viral suppression, all clones are unique, so N is equivalent to the estimate of the total number of latently infected cells at that time. Parameters and likelihoods for each clone are shown in Supplementary Table S5.

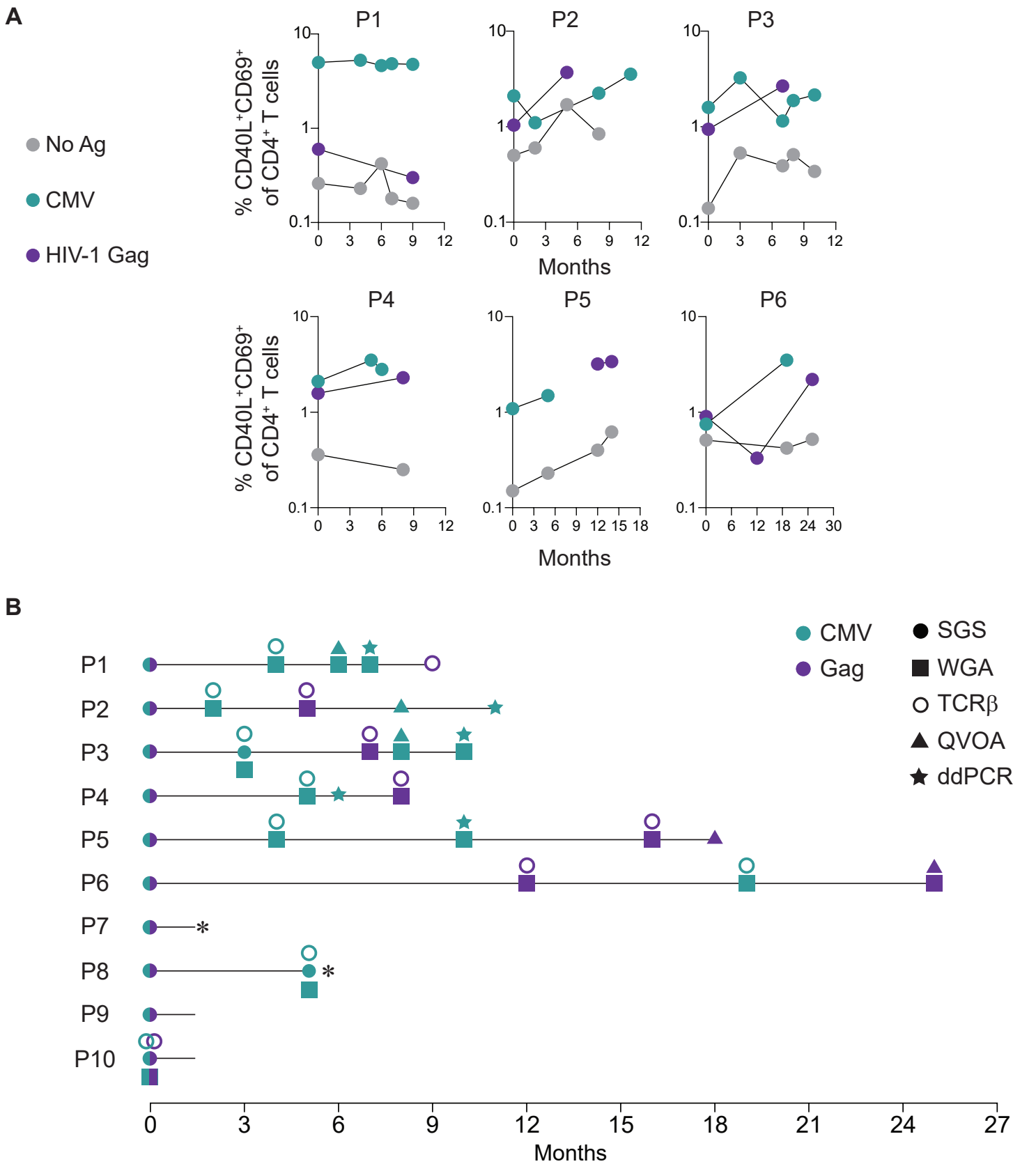
References:

97. Ho YC, Shan L, Hosmane NN, Wang J, Laskey SB, Rosenbloom DI, et al. Replication-competent noninduced proviruses in the latent reservoir increase barrier to HIV-1 cure. *Cell*. 2013;155(3):540-51.
98. Lee GQ, Orlova-Fink N, Einkauf K, Chowdhury FZ, Sun X, Harrington S, et al. Clonal expansion of genome-intact HIV-1 in functionally polarized Th1 CD4+ T cells. *J Clin Invest*. 2017;127(7):2689-96.
99. Anderson EM, and Maldarelli F. The role of integration and clonal expansion in HIV infection: live long and prosper. *Retrovirology*. 2018;15(1):71.
100. Varadarajan J, McWilliams MJ, and Hughes SH. Treatment with suboptimal doses of raltegravir leads to aberrant HIV-1 integrations. *Proc Natl Acad Sci U S A*. 2013;110(36):14747-52.
101. Ode H, Kobayashi A, Matsuda M, Hachiya A, Imahashi M, Yokomaku Y, et al. Identifying integration sites of the HIV-1 genome with intact and aberrant ends through deep sequencing. *J Virol Methods*. 2019;267:59-65.
102. Zhang ZQ, Notermans DW, Sedgewick G, Cavert W, Wietgrefe S, Zupancic M, et al. Kinetics of CD4+ T cell repopulation of lymphoid tissues after treatment of HIV-1 infection. *Proc Natl Acad Sci U S A*. 1998;95(3):1154-9.
103. Besson GJ, Lalama CM, Bosch RJ, Gandhi RT, Bedison MA, Aga E, et al. HIV-1 DNA decay dynamics in blood during more than a decade of suppressive antiretroviral therapy. *Clin Infect Dis*. 2014;59(9):1312-21.
104. Durrett R. *Branching Process Models of Cancer*. Springer; 2015.



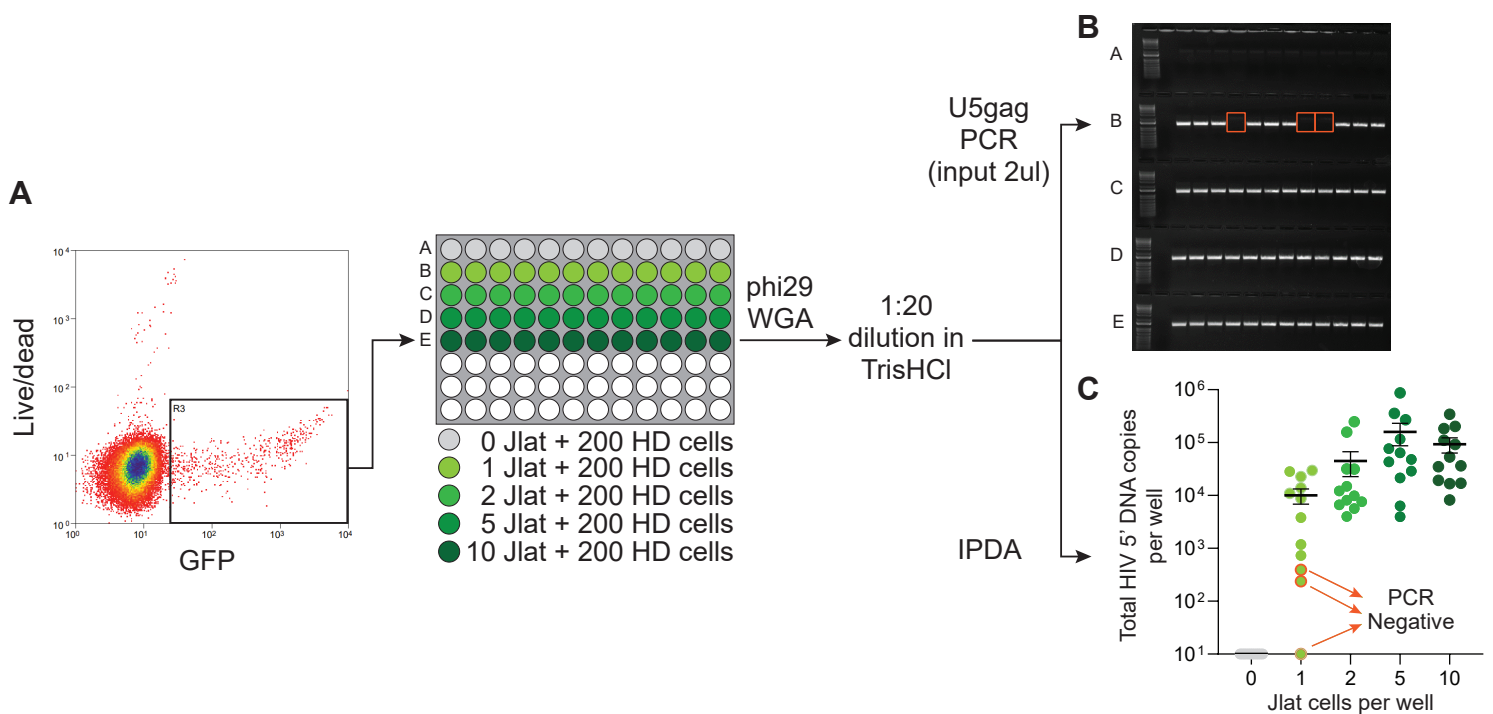
Supplementary Figure S1. Accessing antigen-responding CD4⁺ T cells.

(A) Gating strategy used to isolate CD4⁺ T cells responding to stimulation. Flow data from a representative stimulation of CD8-depleted PBMC with CMV lysate is shown. Non-responding cells gated on CD45RO expression are highlighted in green. (B) Fraction of CD4⁺ T cells responding to the indicated stimulations that are CD45RO^{hi}. Statistical significance was determined by one-way ANOVA test. (C) Frequency of CD4L and CD69 double positive cells among CD4⁺ T cells in response to stimulation of PBMCs from three donors naive for CMV and HIV-1 infection. Numbers in gates indicate percentage of double positive events.

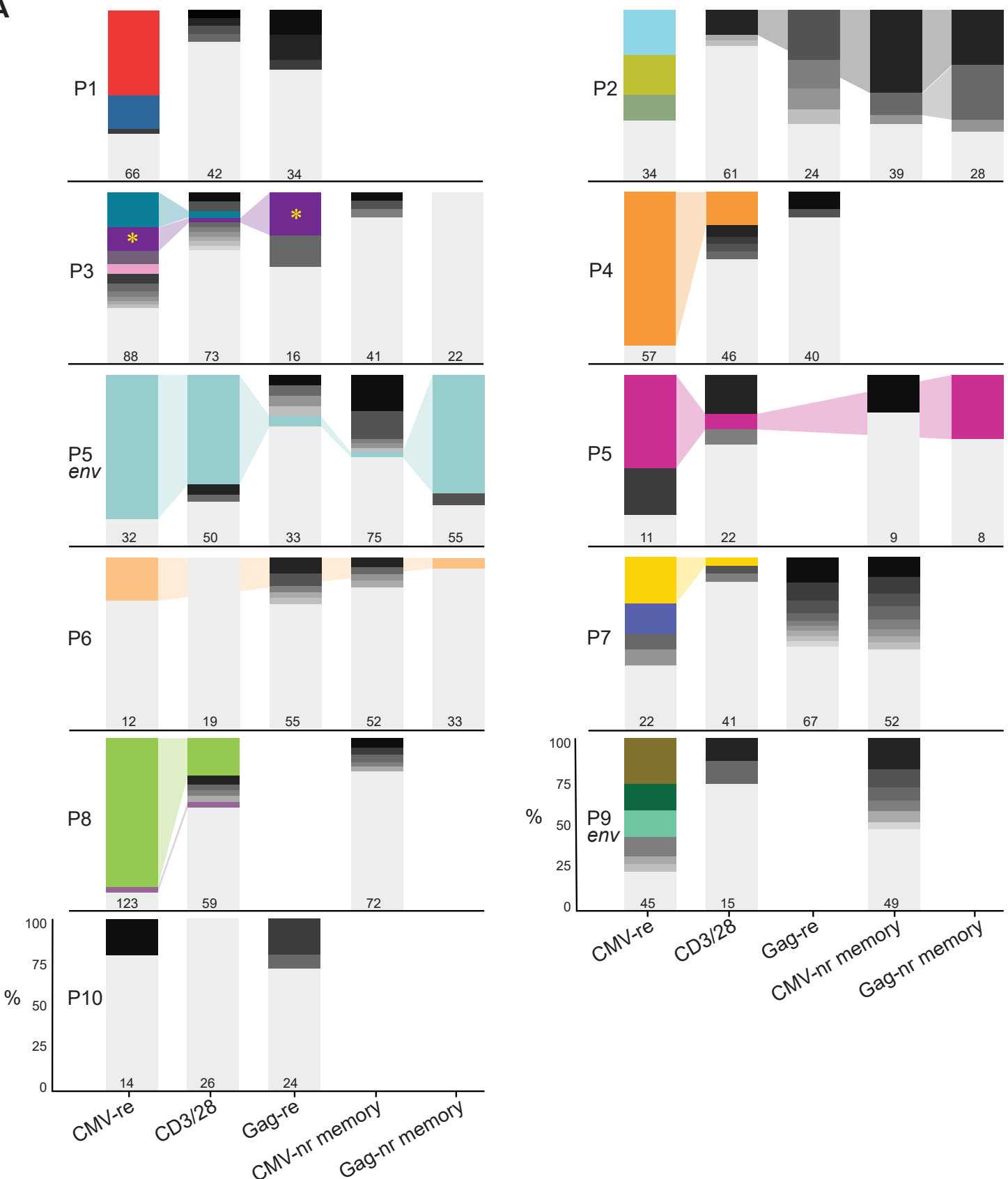


Supplementary Figure S2. Longitudinal sampling schema and experiments performed at each time point.

(A) Frequencies of cells responding to the indicated stimulations in longitudinal samples from 6 participants with at least 3 time points available. (B) Each horizontal line represents one participant. Peripheral blood was collected from longitudinal samples at the indicated time points. Experiments performed on sorted cells are represented as described in the symbol legend. Participants P7 and P8 were lost to follow up (asterisk) due to ART interruption and fatal acute coronary syndrome, respectively.

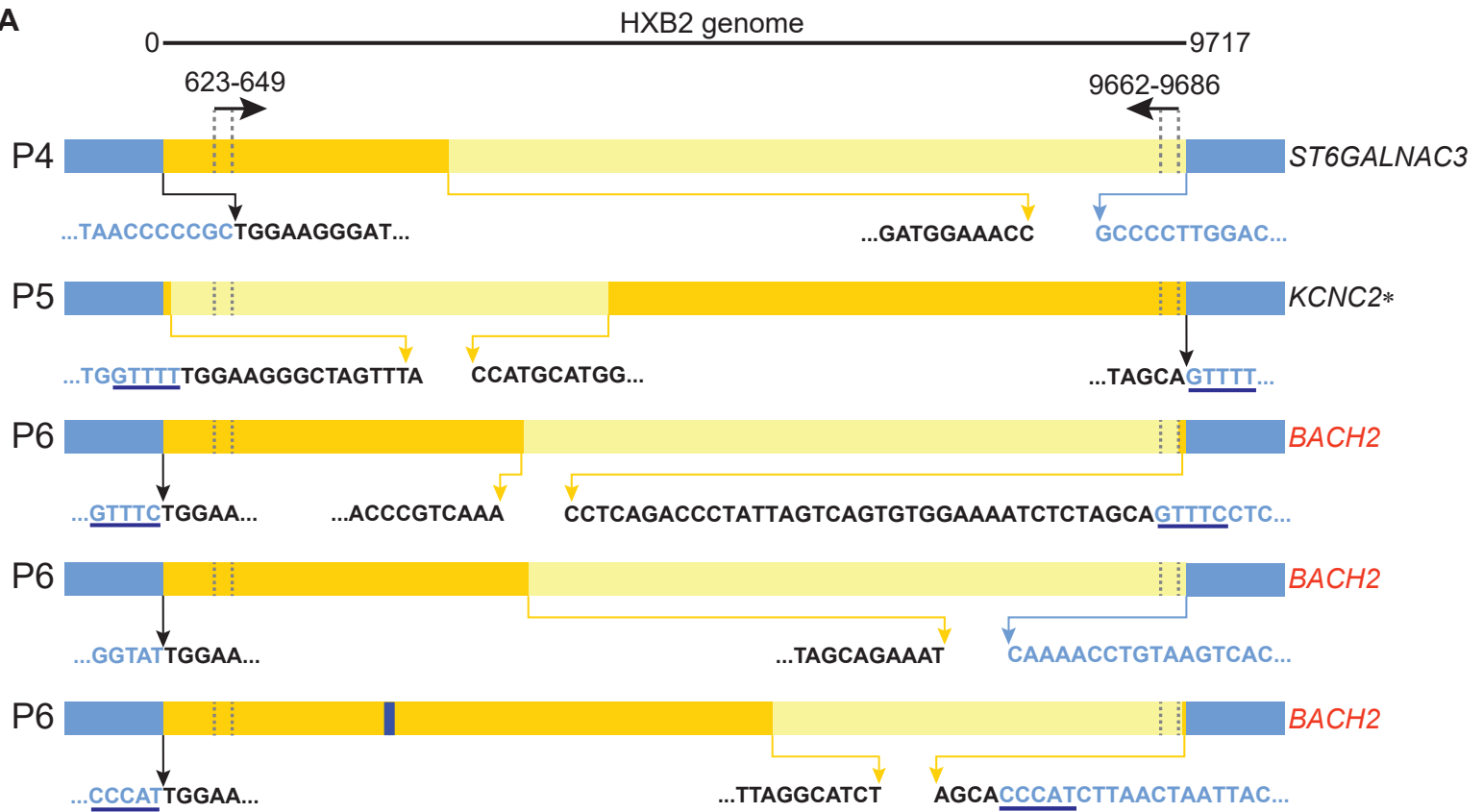


Supplementary Figure S3. Validation experiment of whole genome amplification on sorted JLat cells.
(A) J-Lat cells (clone 10.6) were sorted into wells with 200 CD4⁺ T cells from a healthy donor. Cell pools were subjected to whole genome amplification and a diluted aliquot was used for downstream experiments. **(B)** Electrophoresis gel showing amplification of u5-gag PCR. Reactions lacking expected amplification are highlighted in orange boxes. **(C)** Quantification of 5' HIV genome by IPDA from whole genome amplified wells. Each dot represents the estimate of total HIV genome copies per well. Horizontal bars show mean and standard error of the mean.

A

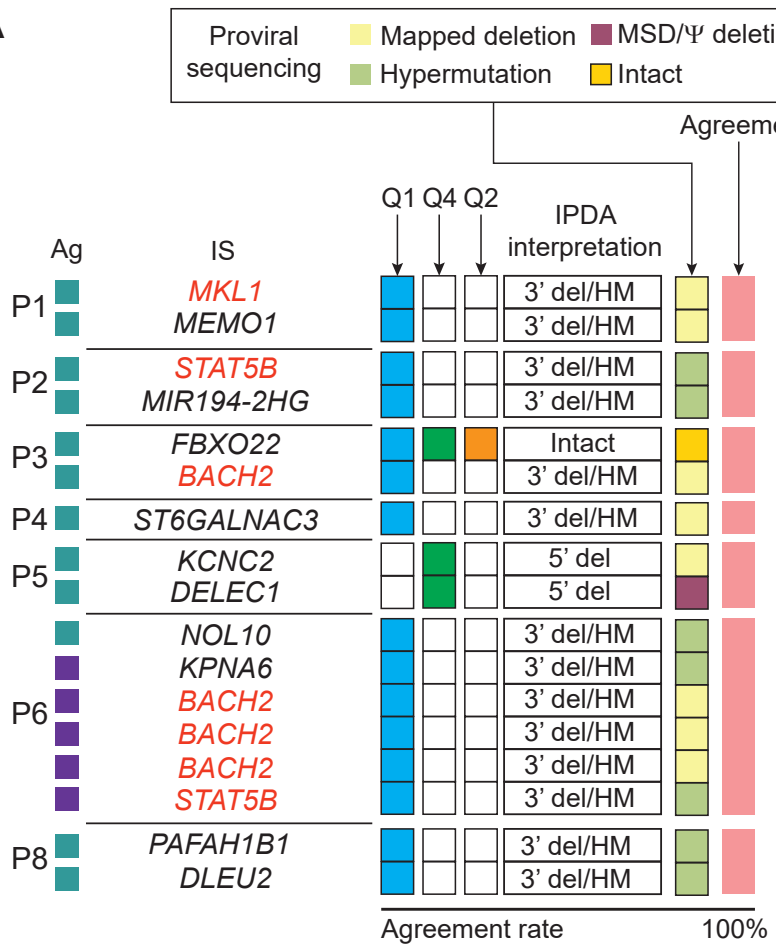
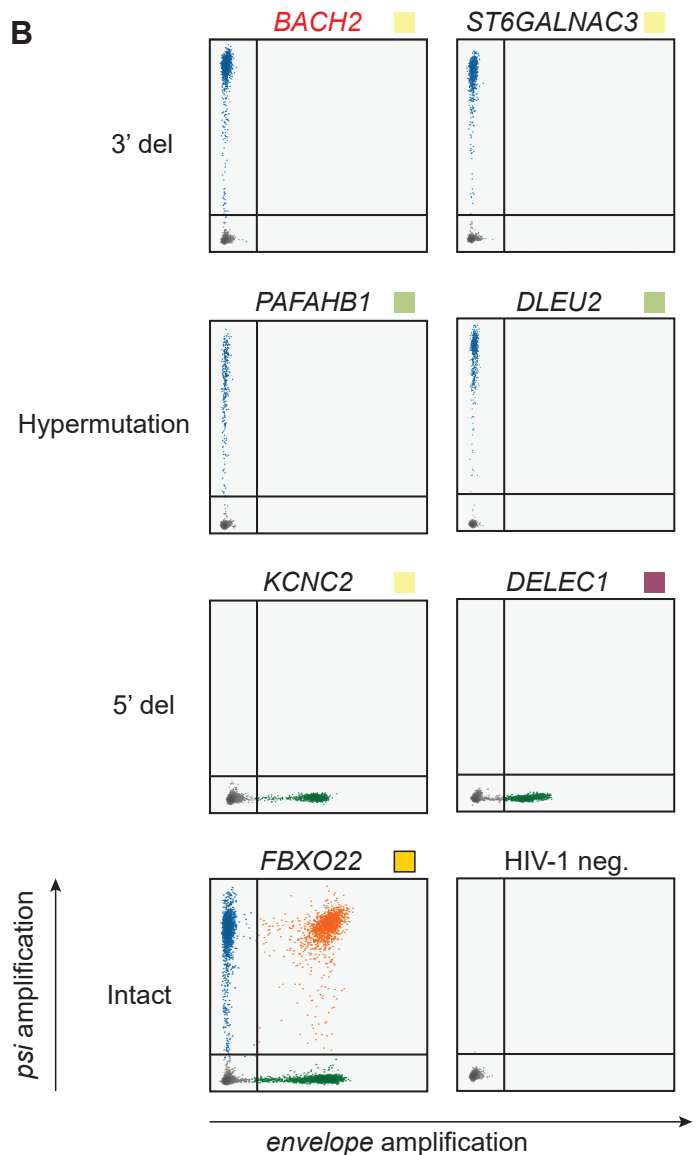
Supplementary Figure S4. Summary of identical HIV-1 DNA single genome sequences recovered from sorted cells.

(A) Stacked bar graphs represent proviral variants ranked by frequency. Variants identified at least twice are shown in shades of grey; clones of interest are color-coded as in main Figure 2C and D; singletons are shown in light grey at the bottom of the stack; potential clones found across more than one cell fraction are connected with shaded colors; the yellow star symbol highlights a case of a proviral sequences enriched both upon stimulation with CMV and Gag antigens.

A

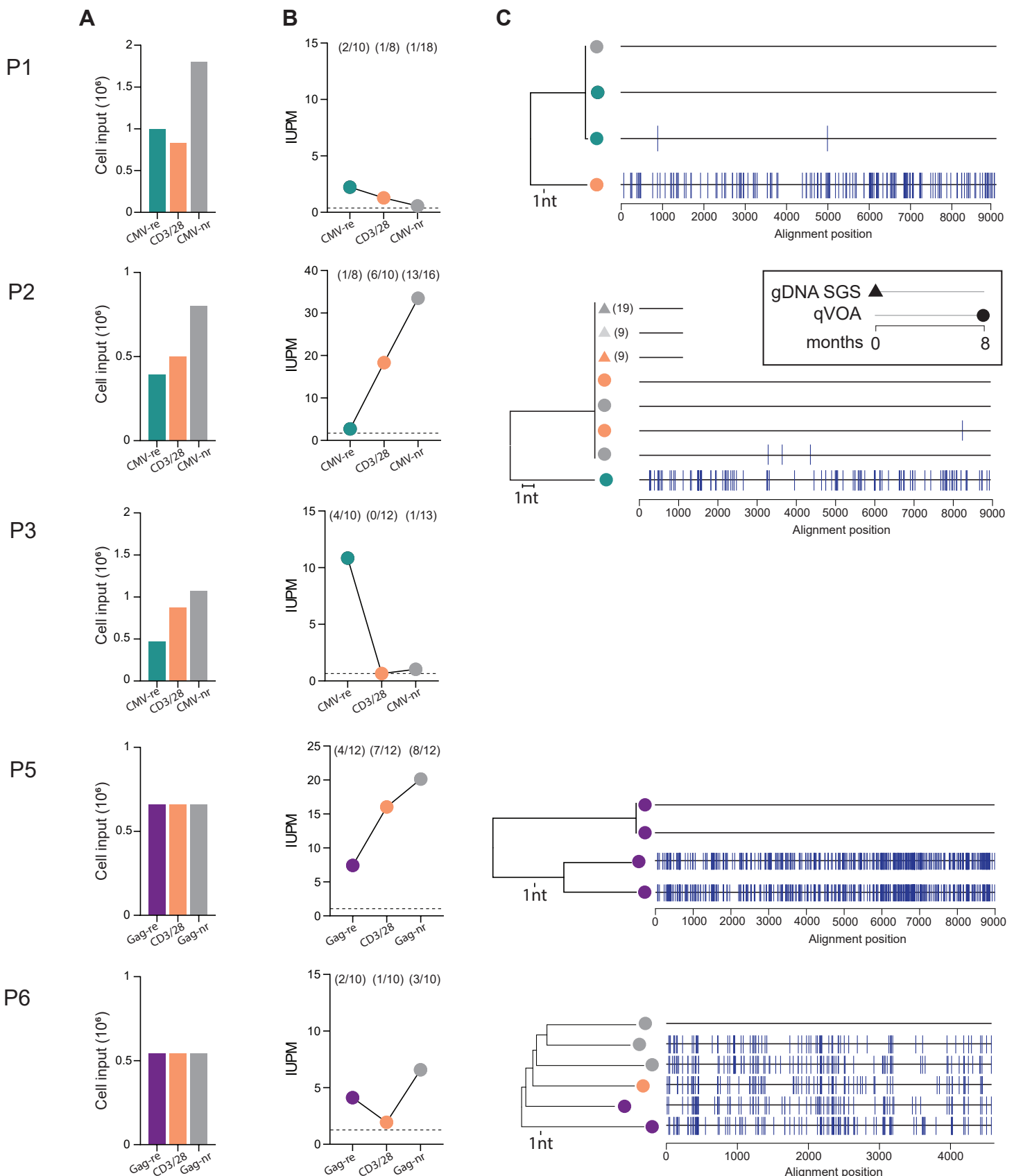
Supplementary Figure S5. Proviral structures with large deletions and aberrant provirus/host junctions.

(A) Horizontal bars show proviral structures as displayed in Figure 3A. Black horizontal arrows and dashed vertical lines show the location of commonly used outer PCR primers (position numbers relative to HXB2 reference). Vertical arrows show the sequence flanking deletions and host-provirus junctions. Nucleotides belonging to the flanking host sequence are colored in blue. Five-nucleotide duplications, result of integrase-mediated insertion, are underscored in dark blue.

A**B**

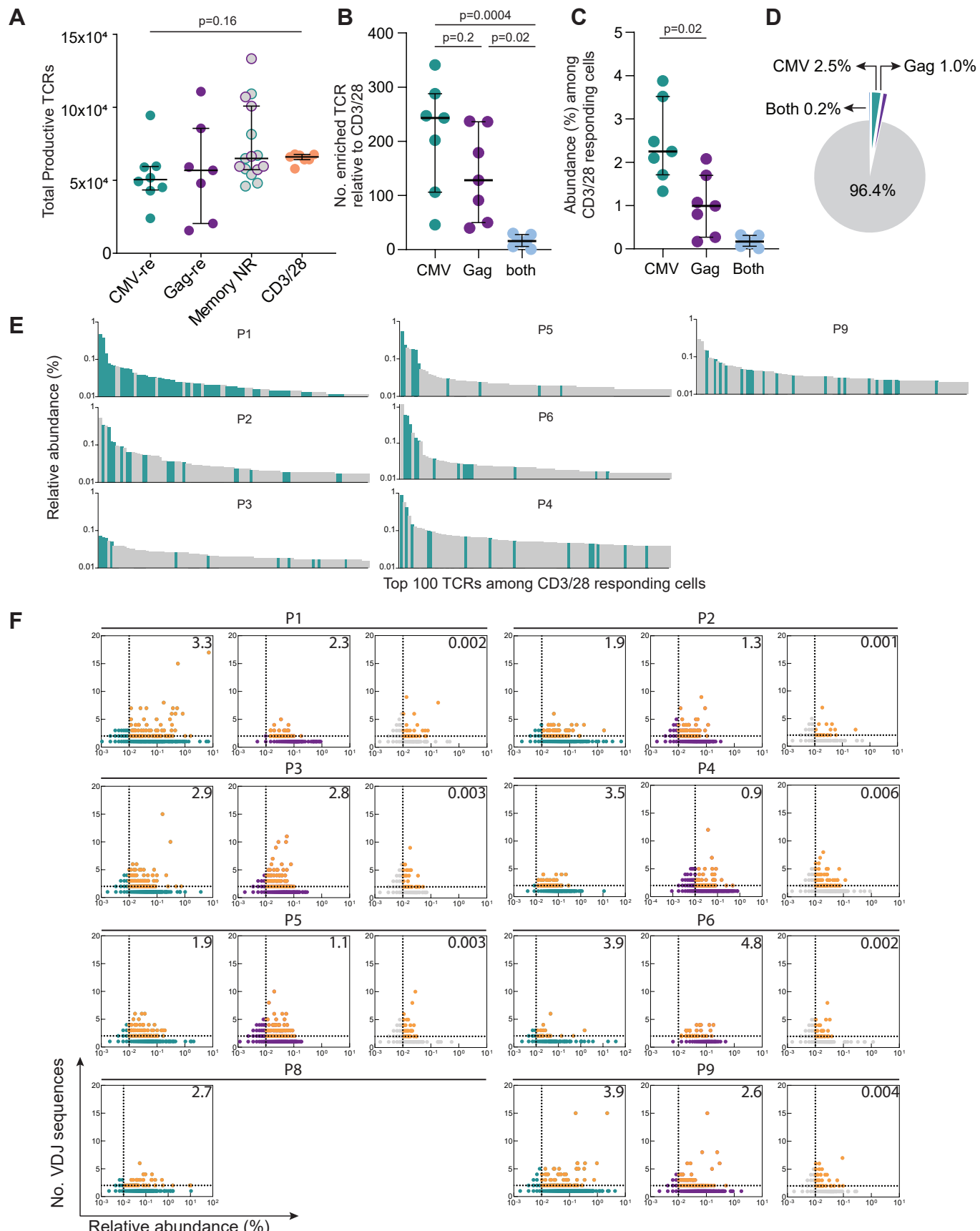
Supplementary Figure S6. Analysis of Intact proviral DNA assay performed on individual proviruses.

(A) Summary of IPDA results from whole genome amplified genomic DNA samples containing individual proviruses (related to Figure 3A). Interpretation of IPDA signal is compared to proviral sequences, with features color-coded according to the boxed legend. Agreement between IPDA and proviral sequencing is highlighted in pink. (C) Examples of two-dimension ddPCR plots from the indicated proviruses with known 3' deletions or hypermutation, 5' deletions or small major splice donor/packaging signal defects, and one intact provirus.



Supplementary Figure S7. Quantitative viral outgrowth assay data from sorted CD4⁺ T cells.

(A) CD8-depleted PBMCs were stimulated as in the previous experiments (P1, P2, P3 with CMV, P4 and P5 with Gag, respectively) and the sorted antigen-responding cells were immediately used as input for the quantitative viral outgrowth assay (qVOA). The number of cells used as input for qVOA experiments for each participant are displayed in bar graphs. **(B)** Frequency of cells with inducible replication-competent proviruses in IUPM from each sorted cell fraction. Numbers in parentheses indicate the number of p24-positive wells out of all replicates performed for each condition. **(C)** Neighbor-Joining (NJ) trees of sequences from p24-positive wells and highlighter plots showing mismatches relative to the top sequence in the tree. In participants P1, P5 and P6, the NJ tree was build based with the same sequences used for the highlighter plot. In P2, NJ tree is based on u5-gag sequences. Source and time point of sequences are described in the insert. Sequence analysis for participant P3 is shown in Figure 3E.

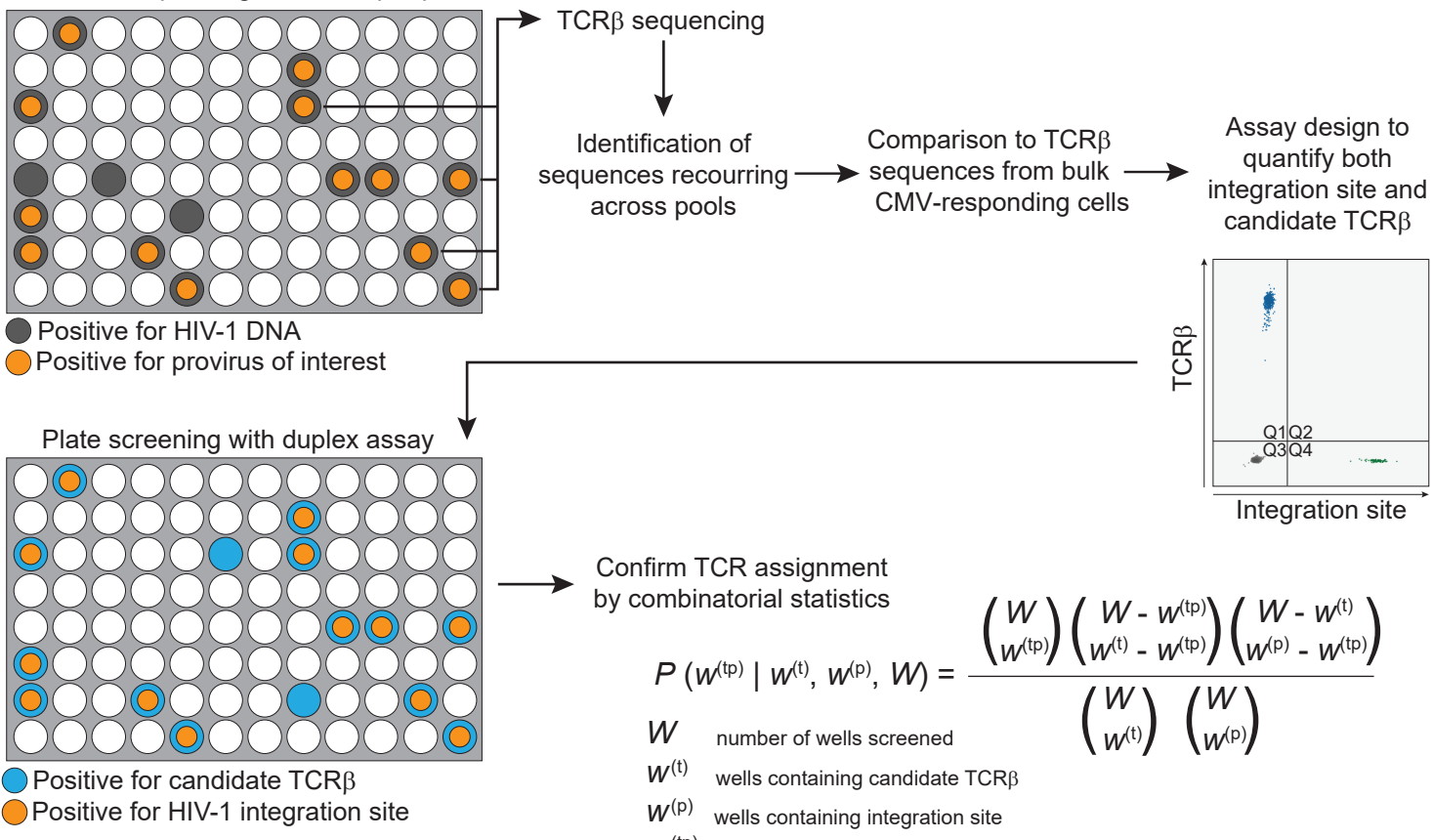


Supplementary Figure S8. Additional analyses on TCR sequences related to Figure 4.

(A) Total productive TCR sequences recovered from sorted cells. Grey circles indicate CD45ROhi cells non responding to either CMV or Gag stimulation (teal and purple border, respectively) (B) Number of TCR sequences from CD3/CD28-responding cells with a significantly higher abundance in CMV- or Gag-responding cells, or both. Horizontal bars show median and interquartile values. Statistical significance was determined using a one-way ANOVA. (C) Relative abundance (%) of TCR sequences enriched in antigen-responding cells among cells activated with a nonspecific stimulation. (D) CMV- and Gag-responding cells represent only a small fraction of all CD3/CD28-responding cells (mean values) (E) Relative abundance (%) of the top 100 clones from CD3/CD28-responding cells. Clones significantly enriched in CMV-responding cells are highlighted in teal. (F) Unique and degenerate CDR3 β sequences were plotted against their relative productive abundance. Degenerate CDR3 β sequences with a sum productive abundance higher than 0.01% are highlighted in orange (their cumulative abundance is indicated in the right upper quadrant).

A

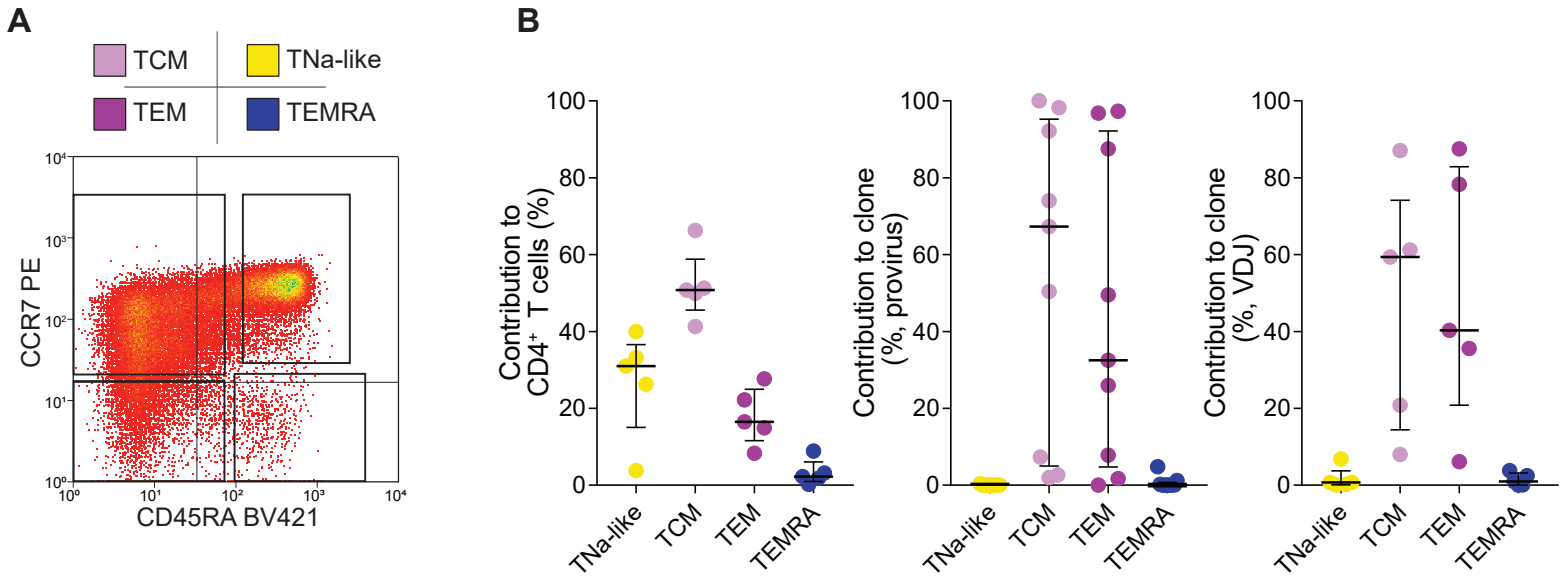
Whole genome amplification of CMV-responding cells, 300 per pool

**B**

Participant ID	TCR β	Provirus	Cells per well	W	$w^{(t)}$	$w^{(p)}$	$w^{(tp)}$	P	Provirus:TCR ratio (WGA)	Provirus:TCR ratio (ddPCR)
P1	CASIGSSAFF	MKL1	100	92	41	7	7	2.5×10^{-3}	0.17	0.14
			300	90	75	15	15	0.049	0.20	
P3	CASSYSTGITEAFF	FBXO22	200	96	16	3	3	3.9×10^{-3}	0.19	0.15
			400	93	23	6	5	3.0×10^{-3}	0.22	
P4	CASSLLTAATNEKLFF	ST6GALNAC3	20	90	5	5	5	2.2×10^{-8}	1.00	0.72
			60	96	10	5	5	4.0×10^{-6}	0.50	
P5	CASSLSGTENSPLHF	KCNC2	15	86	15	12	8	4.0×10^{-5}	0.53	0.93
		CSARATTGELFF	30	92	37	42	33	1.0×10^{-10}	0.89	
P6	CSVARQGAVYEQFF	BACH2.c1	100	96	7	7	7	8.3×10^{-11}	1.00	na
	CASSITGVGGQPQHF	BACH2.c2	100	95	6	5	5	1.0×10^{-7}	0.83	na
	CSVPGLGAEAFF	BACH2.c3	100	95	4	4	4	3.1×10^{-7}	1.00	na

Supplementary Figure S9. Pairing of TCR β sequences and proviruses belonging to the same clonotype.

(A) Experimental approach to pair TCR sequences and proviruses belonging to the same antigen-responding clone. A representative example from participant P5 is shown (CSARATTGELFF-DELEC1 pair). Whole genome amplified cell pools sharing identical proviral sequences and integration sites are subjected to TCR sequencing. Shared TCR sequences are identified and compared to TCR repertoire from bulk antigen-responding cells. If a unique TCR sequence is identified, the pair is confirmed by duplex ddPCR assays designed to amplify both the TCR and the integration site (see methods for details). For each potential TCR β -provirus pair, we screened one or more plates with pools of antigen-reactive cells subjected to WGA and recorded the pattern of occurrence of wells positive for TCR and integration sites. We then computed a P value for the observed number of shared wells, implementing the calculations described by Howie *et al.*(56) (B) Confirmed TCR β -provirus pairs and P values supporting that their pattern of co-occurrence is driven by chance. Of note, the provirus:TCR ratios inferred by the occurrence pattern correlate with the ratios calculated by ddPCR in antigen-responding cells (Figure 5C).



Supplementary Figure S10. Contribution of CD4⁺ T cell subsets to antigen-responsive clonotypes carrying HIV proviruses.

(A) Representative experiment and sorting strategy to isolate CD4⁺ T cell subsets previously gated on single, live, CD14⁻CD16⁻CD20⁻, CD3⁺CD4⁺ cells. (B) Relative contribution (%) of CD4⁺ T cell subsets to total CD4⁺ T cells (left panel) and to proviral copies (center panel) and VDJ rearrangement copies (right panel) of antigen-responsive HIV-1-infected clones.

Supplementary Table S1. Participant characteristics.

Participant ID	Sex	Race	Age	HIV-RNA pre ART (log ₁₀ cps/mL)	HIV-RNA current (log ₁₀ cps/mL)	CD4 ⁺ T cells nadir (cells/mm ³)	CD4 ⁺ T cells current (cells/mm ³)	CD4 ⁺ T cell recovery (cells/mm ³)	Years since HIV-1 diagnosis	Years on ART ^a	Years with <50 HIV-RNA cps/mL ^b	Current ART Regimen ^c
P1	Male	White	56	5.1	<1.3	328	1429	1101	19.8	5.9	4.8	ABC/ 3TC/DTG
P2	Male	AA	57	5.0	<1.3	158	630	472	24.4	24.4	11.9	ZDV/3TC/EFV/ATZ/r
P3	Female	AA	53	4.1	<1.3	320	1224	904	19.5	19.5	10.2	ABC/3TC/DTG
P4	Female	AA	60	4.7	<1.3	159	475	316	13.3	11.0	8.0	TAF/FTC/ATV/c
P5	Male	AA	54	4.7	<1.3	184	1194	1010	21.0	12.9	6.5	TDF/FTC/RPV
P6	Female	AA	39	4.7	<1.3	275	1098	823	25.4	6.4	6.1	ABC/3TC/DTG
P7	Female	AA	59	4.9	<1.3	81	654	573	24.4	8.8	4.4	ETV/RAL/DRV/r
P8	Male	White	63	5.5	<1.3	41	407	366	16.9	16.5	16.2	TAF/FTC/RPV
P9	Male	White	65	4.5	<1.6	105	518	413	28.7	28.0	11.8	TAF/FTC/RPV/DTG
P10	Male	White	59	5.9	<1.6	205	516	311	28.4	27.8	7.9	ABC/3TC/DTG
Median			58	4.8	<1.3	171.5	642	522.5	22.7	14.7	7.9	
IQR			53.7-60.	4.6-5.2		99-286	505.8-1202	353.5-930.5	18.8-26.1	8.2-25.5	5.7-11.8	

^aYears since the beginning of first ART regimen

^bYears of stable suppression with plasma HIV-RNA below limit of detection of clinical assays

^cAntiretroviral drug abbreviations: ABC (abacavir); ATV/r (atazanavir/ritonavir); ATV/c (aaazanavir/cobicistat); DRV/r (darunavir/ritonavir); DTG (dolutegravir); EFV (efavirenz); ETV (etravirine); FTC (emtricitabine); TDF (tenofovir disoproxil fumarate); RAL (raltegravir); ZDV (zidovudine); 3TC (lamivudine)

Supplementary Table S2. Single genome sequences and oligoclonality of proviral populations from sorted CD4+ T cells.

Participant ID	Amplicon	CMV-stim CD40L+CD69+CD4+ cells			Gag-stim CD40L+CD69+CD4+ cells			CD3/28-stim CD40L+CD69+CD4+ cells			CMV non responding CD45RO ^{hi} CD4+ cells			Gag non responding CD45RO ^{hi} CD4+ cells		
		Total	Identical (%)	Gini	Total	Identical (%)	Gini	Total	Identical (%)	Gini	Total	Identical (%)	Gini	Total	Identical (%)	Gini
P1	<i>u5-gag</i>	66	48 (73)	0.64	34	12 (35)	0.25	42	8 (19)	0.09						
P2	<i>u5-gag</i>	34	22 (65)	0.48	24	16 (67)	0.41	61	13 (21)	0.16	39	26 (67)	0.55	28	20 (71)	0.51
P3	<i>u5-gag</i>	88	60 (68)	0.50	16	7 (44)	0.28	73	25 (34)	0.18	41	6 (15)	0.07	22	0 (0)	0.00
P4	<i>u5-gag</i>	57	51 (89)	0.77	40	6 (15)	0.10	46	18 (39)	0.27						
P5	<i>env</i>	33	28 (85)	0.70	33	10 (30)	0.13	50	37 (74)	0.64	75	36 (48)	0.38	55	42 (76)	0.68
P5	<i>u5-gag</i>	11	9 (82)	0.43				22	9 (41)	0.25	9	2 (22)	0.11	8	3 (38)	0.24
P6	<i>u5-gag</i>	12	3 (25)	0.16	55	15 (27)	0.17	19	0 (0)	0.00	52	9 (17)	0.09	33	2 (6)	0.03
P7	<i>u5-gag</i>	22	14 (64)	0.37	67	35 (52)	0.35	41	6 (15)	0.07				52*	28 (54)*	0.32*
P8	<i>u5-gag</i>	123	111 (90)	0.83				59	24 (41)	0.29	72	14 (19)	0.12			
P9	<i>env</i>	45	35 (78)	0.51				15	4 (27)	0.12	49	26 (53)	0.36			
P10	<i>u5-gag</i>	14	3 (21)	0.14	24	7 (29)	0.20	26	0 (0)	0.00						
Total		505	384 (76)		293	108 (37)		454	144 (32)		337	119 (35)		146	67 (46)	
Average		46	35 (67)	0.50	37	14 (37)	0.24	41	13 (28)	0.19	48	17 (34)	0.24	29	13 (24)	0.29

* CMV and Gag non responding CD45RO^{hi} CD4+ cells were pooled, and excluded from calculations

Supplementary Table S3. Integration site analysis of HIV-1-infected antigen-responding clones.

Sample			Provirus							Host gene					
Participant ID	Antigen	Time point (months) ^a	Provirus ID	Chr.	Position ^b	5nt duplication ^c	Host junction recovered	Strand	Orientation relative to gene	Method ^d	Gene symbol ^e	Gene ID	Gene transcription orientation	Intron/exon/ distance ^f	Identified before (ref) ^g
P1	CMV	0,4,6,7	1.c.mkl1	22	40557594	GTCTT	5', 3'	-	same	B, C	MKL1 ~	57591	-	intron 2	8, 9, 10, 12
	CMV	0,4,6	1.c.memo1	2	31948508	ATTTC	5', 3'	-	same	B, C	MEMO1	51072	-	intron 1	12
P2	CMV	0,2,11	2.c.stat5b	17	42241492	CTCCA	5', 3'	-	same	A, C	STAT5B ~	6777	-	intron 1	8, 9, 10, 47
	CMV	0,2	2.c.ddi2	1	15658310	GGACC	5'	-	opposite	A	DDI2	84301	+	intron 9	12
	CMV	0,2,11	2.c.hivep3	1	41985926	AATAT	5'	+	opposite	A, C	HIVEP3 ~	59269	-	intron 1	8, 10, 12
	CMV	0,2	2.c.mir194	11	64885345	CCAAT	3'	+	opposite	A	MIR194-2HG	105369343	-	ig, 3112	
P3	CMV	0,3,7,8,10	3.c.fbxo22	15	75914981	AAAAC	5', 3'	-	opposite	A, B, C	FBXO22	26263	+	intron 4	12
	CMV	0,7	3.c.gdap2	1	117864268	CTTCC	5', 3'	+	opposite	A, C	GDAP2	54834	-	exon 14	12
	CMV	0,3,7,8,10	3.c.ccnl2	1	1390336	CTTTT	5'	+	opposite	A	CCNL2	81669	-	intron 8	10, 12
	CMV	0,3,7,8,10	3.c.bach2	6	90052250	GCTTG	5', 3'	-	same	A, B, C	BACH2 ~	60468	-	intron 5	8, 9, 10, 12, 47
P4	CMV	0,5,6	4.c.st6	1	76337191	CCCGC/ab	5', 3'	+	same	B, C	ST6GALNAC3	256435	+	intron 2	8, 12
P5	CMV	0,4,10	5.c.kcnc2	12	74917002	GTTTT	5', 3'	+	opposite	A, B, C	KCNC2	3747	-	ig, 123075	
	CMV	0,4,10	5.c.dec1	9	114949387	GGTGT	5', 3'	-	opposite	A, B, C	DELEC1 ~	50514	+	intron 2	
P6	CMV	0,19	6.c.nol2	2	10680857	CACTC	3'	+	opposite	B, C	NOL10	79954	-	intron 3	8
	Gag	0,12,25	6.g.bach2.c1	6	90230775	GTTTC	5', 3'	-	same	A, B, C	BACH2 ~	60468	-	intron 3	8, 9, 10, 12, 47
	Gag	0,12,25	6.g.bach2.c2	6	90063562	GGTAT/ab	5', 3'	-	same	A, B, C	BACH2 ~	60468	-	intron 5	8, 9, 10, 12, 47
	Gag	0,12,25	6.g.bach2.c3	6	90037792	CCCAT	5', 3'	-	same	A, B, C	BACH2 ~	60468	-	intron 5	8, 9, 10, 12, 47
	Gag	0,12,25	6.g.kpna2	1	32131583	TATAT	5', 3'	-	opposite	A, B, C	KPNA6	3838	+	intron 1	10
	Gag	0,12,25	6.g.cramp1	16	1650160	AATAC	5', 3'	-	opposite	A, C	CRAMP1	57585	+	intron 6	9, 12
	Gag	0,12,25	6.g.stat5b	17	42234035	ATAAC	5', 3'	-	same	A, C	STAT5B ~	6777	-	intron 1	9, 47
P8	CMV	0,5	8.c.paf	17	2671849	GCGGG	5'	-	opposite	A	PAFAH1B1	5048	+	intron 6	8, 12
	CMV	0,5	8.c.dle	13	50070306	TAAAC	5', 3'	+	opposite	A	DLEU2 ~	8847	-	intron 4	12

a Proviruses detected by sequence identity or integration site

b Number refers to the third nucleotide of the duplication, using GRCH38/hg38 assembly

c Insertion junction not at the beginning or end of the LTR is defined as aberrant (ab)

d A (INSPIRED, LM-PCR plus paired-end sequencing), B (Lenti-X, LM-PCR plus direct Sanger), C (ISS-PCR, standard or dd PCR using primers across the integration junction)

e Genes previously linked to HIV-1 persistence are highlighted in red; ~ indicates the gene is a cancer related gene

f If integration site is intergenic (ig) nucleotide distance from nearest gene is provided

g Data from NCI Retrovirus Integration Database⁸⁷; only studies on ART-treated individuals were included

Supplementary Table S4. Characteristics of TCR β sequences in clusters shown in Figure 4.

Characteristics of the TCR sequences within clusters displayed in Figure 4. HLA genes with alleles shared among all subjects within a cluster are highlighted in pink. Predicted binding HLA alleles, significantly enriched in subjects within the cluster, are highlighted in yellow.

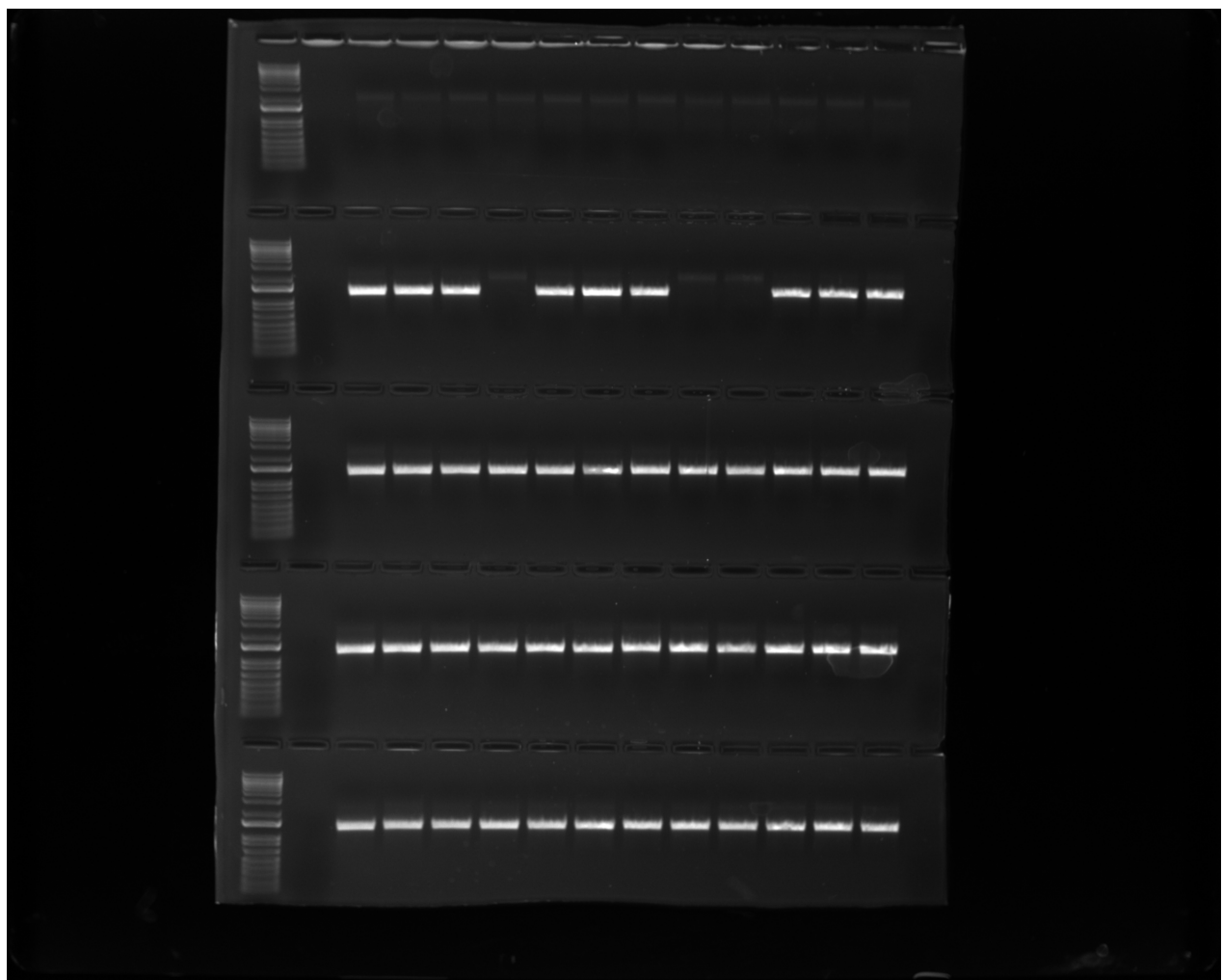
Supplementary Table S5. Likelihoods that clones would reach the observed sizes under a model of homeostatic proliferation.

Clone ID	Time since VL <50cpl/mL (years)	Total size of observed clone	Total divisions needed	Proliferation rate (/year)	Net decay (/year)	Half-life (months)	Probability any clone is at least this big	Net decay (/year)	Half-life (months)	Probability any clone is at least this big
p1.c.mkl1	4.8	1.28×10^7	23.6	10	-0.19	44	0	0	∞	0
				100	-0.19	44	0	0	∞	0
				1000	-0.19	44	0	0	∞	0
p1.c.memo1	4.8	1.42×10^6	20.4	10	-0.19	44	0	0	∞	0
				100	-0.19	44	0	0	∞	2×10^{-127}
p2.c.stat5b	11.9	1.59×10^6	20.6	10	-0.19	44	0	0	∞	0
				100	-0.19	44	0	0	∞	0
				1000	-0.19	44	5×10^{-147}	0	∞	10^{-57}
p2.c.hivep3	11.9	1.18×10^5	16.8	10	-0.19	44	0	0	∞	0
				100	-0.19	44	18^{-107}	0	∞	10^{-41}
				1000	-0.19	44	6×10^{-11}	0	∞	8×10^{-4}
p3.c.bach2	10.2	3.44×10^5	18.4	10	-0.19	44	0	0	∞	0
				100	-0.19	44	0	0	∞	5×10^{-145}
				1000	-0.19	44	4×10^{-33}	0	∞	4×10^{-14}
p3.c.fxbo22	10.2	8.52×10^5	19.7	10	-0.19	44	0	0	∞	0
				100	-0.19	44	0	0	∞	0
				1000	-0.19	44	5×10^{-84}	0	∞	10^{-35}
p4.c.st6	8	2.40×10^7	24.5	10	-0.19	44	0	0	∞	0
				100	-0.19	44	0	0	∞	0
				1000	-0.19	44	0	0	∞	0
p5.c.kcnc2	6.5	4.95×10^7	25.6	10	-0.19	44	0	0	∞	0
				100	-0.19	44	0	0	∞	0
				1000	-0.19	44	0	0	∞	0
p5.c.delec1	6.5	3.19×10^6	21.6	10	-0.19	44	0	0	∞	0
				100	-0.19	44	0	0	∞	3×10^{-212}
				1000	-0.19	44	0	0	∞	

Supplementary Table S7. High resolution HLA genotyping of the study participants.

High resolution HLA typing of participants included in the TCR sequence analyses

Participant ID	A	C	B	DRB1	DRB3	DRB4	DRB5	DQA1	DQB1	DPA1	DPB1
P1	*02:01	*17:03	*41:02	*07:01	*01:01	*01:01		*02:01	*02:02	*01:03	*11:01
	*29:02	*16:01	*44:03	*13:03				*05:05	*03:01	*02:01	*104:01
P2	*02:01	*08:02	*14:02	*01:02	*03:01			*01:01	*05:01	*01:03	*02:01
	*03:01	*07:01	*49:01	*13:02				*01:02	*06:09	*02:01	*17:01
P3	*02:01	*01:02	*27:05	*01:02			*01:01	*01:01	*05:01	*02:01	*01:01
	*68:01	*04:01	*53:01	*15:01				*01:02	*06:02		*11:01
P4	*02:01	*07:02	*07:02	*08:03			*01:01	*06:01	*03:01	*01:03	*104:01
	*68:01	*03:04	*40:01	*15:01				*01:02	*06:02		
P5	*30:01	*04:01	*53:01	*07:01		*01:03		*02:01	*02:02	*02:01	*01:01
	*30:02	*07:01	*57:03	*08:04				*04:01	*03:19		
P6	*26:01	*04:01	*35:01	*11:01	*02:02			*01:02	*06:02	*02:01	*01:01
	*30:02	*18:01	*81:01	*13:04				*05:05	*03:19		*11:01
P8	*03:01	*07:02	*07:02	*07:01		*01:01	*01:01	*02:01	*02:02	*01:03	*02:02
		*07:01	*08:01	*15:01				*01:02	*06:02		*03:01
P9	*11:01	*04:01	*35:01	*08:03				*01:01	*05:01		*04:01
		*15:02	*51:01	*01:03				*06:01	*03:01		



Original electrophoresis gel used in Supplementary Figure S3 panel B